Stability of the Oscillation Mode in a Multiple-Oscillator System

SUSUMU HAMAYA, MEMBER, IEEE

Abstract—By using the Rieke diagram in terms of traveling waves, we discuss the stability conditions for an oscillation mode in a multiple-oscillator system which clearly indicate the reason why it is difficult for a multiple-oscillator system to obtain a single-mode operation. Further, we proposed a combining power system of oscillators which can give a stable operation free from the moding problem. Experimental observations are found to be in good agreement with the conclusions of the analytical approach.

I. Introduction

OVER THE YEARS, there has been great interest in developing techniques for combining power from microwave and millimeter-wave power sources [1]–[9]. Microwave power-combining techniques can be classified into two categories:

1) a number of devices that contribute to the output power in a single circuit [1]–[4],
2) the output powers from a number of oscillators that are summed to produce a higher output power [5]–[7].

Most of the approaches for power combining of solid-state devices belong to the former class because of the ease of attaining single-mode operation [1]–[4]. With the combined oscillator in the latter class it is inherently difficult to control oscillation modes [8]. However, studies of the latter class are important for the purpose of combining oscillators, such as magnetrons and klystrons, and for use with the method in the former class.

In this paper, we clarify why it is difficult for a multiple-oscillator system to control oscillation modes. We then discuss the condition to overcome this difficulty. To this end, in Section II, we transform the Rieke diagram in terms of the power into one in terms of traveling waves. In Section III, we discuss the stability of oscillation in an injection-locked oscillator using the new Rieke diagram. In Section IV, extending the discussion in Section III, we obtain a stability condition for the oscillation mode in the multiple-oscillator system. In Section V, we apply the stability condition to a power-combining system with hybrid couplers.

II. Rieke Diagram in Terms of Traveling Waves

Fig. 1 shows a circuit of the injection-locked oscillator. If a signal is injected with a frequency close to the free-running frequency, the oscillator will be locked to the injection signal. The quantities a and b shown in Fig. 1 will be called, respectively, the output and input waves of the oscillator. We define the inverse reflection coefficient of the oscillator S_G as

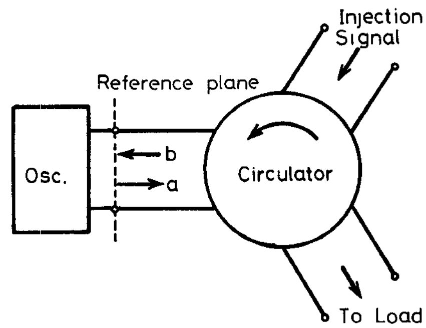

Fig. 1. An equivalent circuit of an injection-locked oscillator with a circulator.

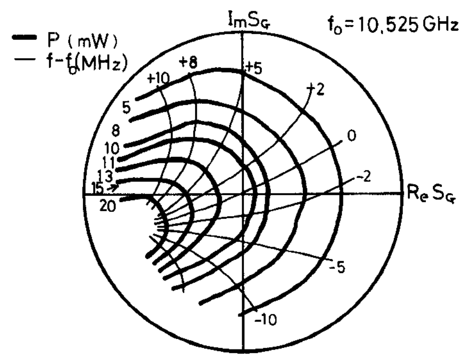

Fig. 2. Measured Rieke diagram of a Gunn oscillator.

$$S_G = b/a \tag{1}$$

where a and b are values at the reference plane in Fig. 1.

Fig. 2 shows the conventional Rieke diagram of a Gunn oscillator on the S_G plane. The constant power contours in Fig. 2 can be transformed into constant amplitude contours of A ($=|a|$) and B ($=|b|$). Using the relation

$$P = A^2 - B^2 \tag{2}$$

we have

$$A^2 = P/(1-|S_G|^2) \tag{3}$$

$$B^2 = |S_G|^2 \cdot P/(1-|S_G|^2) \tag{4}$$

Manuscript received July 30, 1984; revised February 11, 1985.
The author is with Numazu College of Technology, 3600, Ooka, Numazu, 410 Japan.

0018-9480/85/0700-0593$01.00

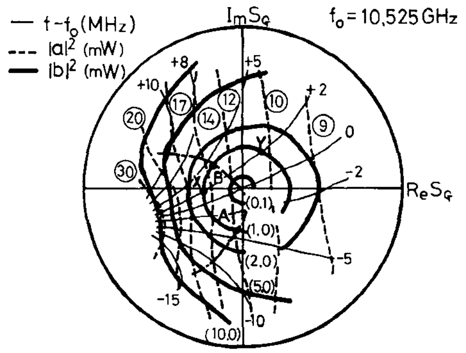

Fig. 3. Rieke diagram in terms of the traveling waves for the same Gunn oscillator as in Fig. 2. $|a|^2$: numbers shown in circles. $|b|^2$: numbers shown in parentheses.

where P, A, and B are values of the oscillator at an operating point S_G. Applying (3) and (4) to the constant power contours in Fig. 2, we obtain constant amplitude contours of the output and input waves, as shown in Fig. 3.

Now we can express S_G as a function of A and an angular frequency ω, i.e.,

$$S_G = S_G^{\langle A \rangle}(A, \omega) \tag{5}$$

or a function of B and ω, i.e.,

$$S_G = S_G^{\langle B \rangle}(B, \omega). \tag{6}$$

In this paper, we use the latter expression because the oscillator in the injection-locked mode is controlled by an input wave [10]. Here, it is assumed that $S_G(B, \omega)$ is an instantaneous function of B. From now on, $S_G^{\langle B \rangle}(B, \omega)$ will be replaced by $S_G(B, \omega)$.

Since we consider a small-signal perturbation in this paper, we can express S_G approximately in the vicinity of an operating point S_o as follows [9], [10]:

$$S_G(B, \omega) = S_o + S_{GBo} \cdot (B - B_o) + S_{G\omega o} \cdot (\omega - \omega_o). \tag{7}$$

The terms on the right-hand side of (7) are the first three terms of the Taylor expansion of $S_G(B, \omega)$ and

$$S_o = S_G(B_o, \omega_o) \tag{8}$$

$$S_{GBo} = (\partial S_G / \partial B) \text{ at } S_o \tag{9}$$

$$S_{G\omega o} = (\partial S_G / \partial \omega) \text{ at } S_o. \tag{10}$$

S_G in square brackets [ ] indicates an operator which is applied to the output wave a. Therefore, $[S_G]$ is interpreted as follows [8], [10]:

$$\begin{aligned} &[S_G(B_o, \omega)] \, \rho \exp((\alpha + j\omega_1)t + j\theta) \\ &\quad = S_G(B_o, \omega_1 - j\alpha) \cdot \rho \exp((\alpha + j\omega_1)t + j\theta) \end{aligned} \tag{11}$$

where ρ, ω_1, θ, and α are constants. This is justifiable since the time derivative is everywhere replaced by multiplication by $j\omega$ in the ac circuit theory.

III. Analysis of Stability of Operating Point

A. Injection-Locked Oscillator

Suppose that the locking has been established in the circuit shown in Fig. 1. Then the corresponding equation is given by

$$[S_G(B_o, \omega)] \, a_o = b_o \tag{12}$$

where

$$\begin{aligned} a_o &= |a_o| \exp(j\omega_o t) \\ b_o &= |b_o| \exp(j\omega_o t + j \operatorname{Arg} S_G(B_o, \omega_0)). \end{aligned} \tag{13}$$

In case $|b_o|^2 = 1$ mW and $f - f_o = +2$ MHz, we may expect that the oscillator is locked at the operating point X or Y, as shown in Fig. 3. On the other hand, in case $|b_o|^2 = 1$ mW and $f - f_o = +5$ MHz, no locking takes place because no operating point which satisfies (12) exists.

Even if an operating point which satisfies (12) exists in Fig. 3, no locking takes place at the operating point, which is unstable for a small perturbation. When b_o is changed by a small amount Δb, the locked-oscillator equation (12) becomes

$$\begin{aligned} &[S_o + S_{GBo} \cdot (|b_o + \Delta b| - |b_o|) + S_{G\omega o} \cdot (\omega - \omega_o)](a_o + \Delta a) \\ &\qquad = b_o + \Delta b. \end{aligned} \tag{14}$$

To determine a behavior of $\Delta a (= \Delta a(t))$, let us express Δa as follows:

$$\Delta a(t) = \Delta a(0) \cdot \exp((\alpha + j(\omega_o + \omega_n))t) \tag{15}$$

where ω_n, as well as the magnitude of Δa, is a slowly varying function of time compared to one RF cycle.

Now, assume that Δb is removed and enquire whether or not Δa decays with time. If it does, such an operating point is stable. When Δb is removed, (14) becomes

$$[(S_o + S_{G\omega o} \cdot (\omega - \omega_o))](a_o + \Delta a) = b_o. \tag{16}$$

If a nonzero Δa exists, substituting (12) into (16), we have

$$(S_o + S_{G\omega o} \cdot (\omega_n - j\alpha)) \cdot \Delta a = 0. \tag{17}$$

Equation (17) determines α for a given ω_n. Referring to (11), we can state the following:

1) When $\alpha > 0$, the operating point is unstable.
2) When $\alpha < 0$, the operating point is stable.
3) When $\alpha = 0$, the operating point is stable; however, in this case, the FM noise becomes extremely large [9], [10].

From (17), the operating point S_o is stable provided the origin of the Rieke diagram is located on the left-hand side of the vector direction of $S_{G\omega o}$, which originates at the point S_o. Therefore, in Fig. 4, for example, operating points S_{o1} and S_{o2} are stable; on the other hand, operating points S_{o3} and S_{o4} are unstable. Then, in Fig. 3, the operating point Y is stable and X is unstable. From the above discussion, the points of contact between the constant contour of a frequency and an input-wave amplitude form a boundary between the stable and the unstable regions of the operating point. In Fig. 3, the dashed-dotted line represents a boundary line obtained in this way.

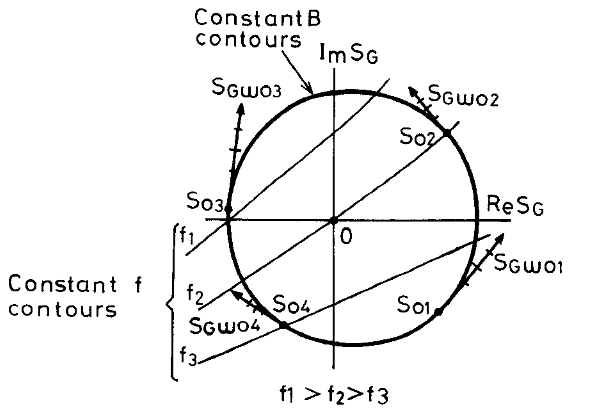

Fig. 4. Explaining the stability of the operating point.

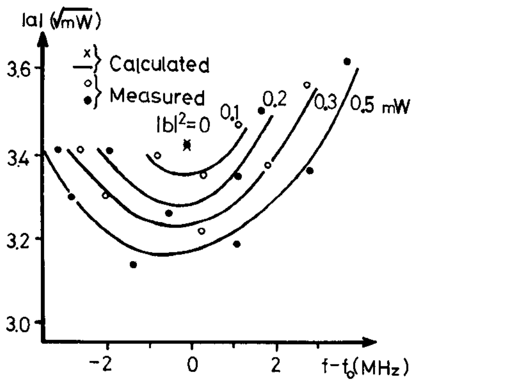

Fig. 5. The output-wave amplitude versus the injection frequency.

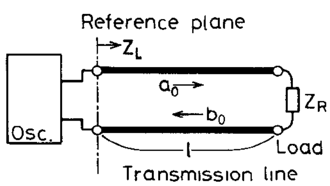

Fig. 6. Free-running oscillator terminated with a load.

When necessary, we express the operating point $S_G(B_o, \omega_o)$ in the stable region as $S_G^{\langle s\rangle}(B_o, \omega_o)$ and in the unstable region as $S_G^{\langle u\rangle}(B_o, \omega_o)$.

In the circuit as shown in Fig. 1, suppose that the frequency of the input wave is swept with a constant amplitude. When $|b_o|^2 = 1.0$ mW, for example, the operating point moves from A through Y to B along the constant amplitude contours of the input wave in Fig. 3. A solid line in Fig. 5 shows the locking range and the output-wave amplitude variation as the frequency of an input wave is swept, which are predicted from Fig. 3. Fig. 5 shows that the analytical results agree well with experimental results for various values of $|b_o|^2$.

B. Free-Running Oscillator Terminated with a Load

Fig. 6 shows a diagram of the free-running oscillator terminated with a load. Here, the input wave $b_o(=B_o \cdot \exp(j\omega_o t + j\xi_o))$ is the reflected wave from the load. When the oscillator in Fig. 6 is in the steady state at the operating point $S_o(=S_G(B_o, \omega_o))$, the corresponding equation to (12) is given by

$$[S_G(B_o, \omega) - S_L(\omega)]\, a_o = 0 \qquad (18)$$

where $S_L(\omega)$ is the reflection coefficient looking into the load from the reference plane shown in Fig. 6. From (18), we obtain

$$S_o = S_G(B_o, \omega_o) = S_L(\omega_o). \qquad (19)$$

In the vicinity of the operating point S_o, by the use of the Taylor expansion, $S_L(\omega)$ is approximated as follows:

$$S_L(\omega) = S_o + S_{L\omega o} \cdot (\omega - \omega_o). \qquad (20)$$

As the corresponding equations to (16) and (17), we have

$$[S_G(B_o, \omega) - S_L(\omega)](a_o + \Delta a) = 0 \qquad (21)$$

$$(S_{G\omega o} - S_{L\omega o}) \cdot (\omega_n - j\alpha) \cdot \Delta a = 0. \qquad (22)$$

Equation (22) is equivalent to (17) in which S_o and $S_{G\omega o}$ are replaced by 0 and $S_{G\omega o} - S_{L\omega o}$. Therefore, referring to discussions in Section III, we see that in the analysis of the stability, the oscillator in the circuit as shown in Fig. 6 is equivalent to the free-running oscillator ($S_o = 0$) for which $S_{G\omega o}$ is replaced by $S_{G\omega o} - S_{L\omega o}$.

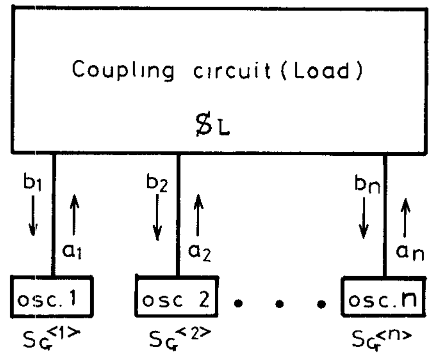

Fig. 7. Power-combining system of n oscillators.

IV. Stability of the Oscillation Mode in the Multiple-Oscillator System

In a power-combining system with n oscillators, there exist more than n oscillation modes in general. Here, we study the stability of an oscillation mode.

Fig. 7 shows a power-combining system with n oscillators. $\mathbf{S}_L(\omega)$ represents the scattering matrix of the coupling circuit at the reference plane, and $\mathbf{S}_G(B, \omega)$ is that of the oscillators. $\mathbf{S}_G(B, \omega)$ is a diagonal matrix whose ith diagonal component equals $S_G^{\langle i\rangle}(B_i, \omega_o)$, where the superscript $\langle i\rangle$, as well as the subscript i, represents the value of the ith oscillator.

Suppose that the locking has been established at ω_o in the combining power system shown in Fig. 7; then the equation of the circuit is given by

$$[\mathbf{S}_G(B_o, \omega_o) - \mathbf{S}_L(\omega_o)]\, \mathbf{a}_o = \mathbf{0} \qquad (23)$$

where $\mathbf{a}_o$ represents an output-wave vector, i.e.,

$$\mathbf{a}_o = (a_{o1}, a_{o2}, \cdots, a_{on})^T. \qquad (24)$$

Operating points $S_G^{\langle i\rangle}(B_{oi}, \omega_o)$, where $i = 1, 2, \cdots, n$, are given by calculating the following equation:

$$\det[\mathbf{S}_G(B_o, \omega_o) - \mathbf{S}_L(\omega_o)] = 0. \qquad (25)$$

Let $\mathbf{x}_k$ be the eigenvector of the matrix in (23) and $\lambda_k(\omega_o)$

be the corresponding eigenvalue. Then we can rewrite $\boldsymbol{a}_o$ as follows:

$$\mathbf{a}_o = \sum_{k=0}^{n-1} a_{ok} \cdot \boldsymbol{x}_k \exp(j\omega_{ok} t) \tag{26}$$

where a_{ok} is a constant indicating the output-wave amplitude and ω_{ok} is the root of $\lambda_k(\omega_o) = 0$. Now, assume that the input-wave vector is perturbed by a small amount $\Delta \boldsymbol{b}$, where

$$\Delta \boldsymbol{b} = (\Delta b_1, \Delta b_2, \cdots, \Delta b_n)^T.$$

Then the corresponding equation of (23) is given by

$$[\boldsymbol{S}_G(\boldsymbol{B}_o + \Delta \boldsymbol{B}, \omega) - \boldsymbol{S}_L(\omega)](\boldsymbol{a}_o + \Delta \boldsymbol{a}) = \Delta \boldsymbol{b} \tag{27}$$

where $\Delta \boldsymbol{a} = (\Delta a_1, \Delta a_2, \cdots, \Delta a_n)^T$.

When $\Delta \boldsymbol{b}$ is taken away, (27) becomes

$$[\boldsymbol{S}_G(\boldsymbol{B}_o, \omega) - \boldsymbol{S}_L(\omega)](\boldsymbol{a}_o + \Delta \boldsymbol{a}) = \mathbf{0}. \tag{28}$$

From (23) and (27), we obtain

$$[\boldsymbol{S}_N(\omega)] \Delta \boldsymbol{a} = \mathbf{0} \tag{29}$$

where

$$[\boldsymbol{S}_N(\omega)] = [\boldsymbol{S}_G(\boldsymbol{B}_o, \omega) - \boldsymbol{S}_L(\omega)]. \tag{30}$$

Let $\boldsymbol{x}_k$ be the eigenvector of $\boldsymbol{S}_N(\omega)$ and let $\mu_k(\omega)$ be the corresponding eigenvalue. Note that the eigenvectors of $\boldsymbol{S}_N(\omega)$ are equivalent to those of the matrix in (23). Then we can rewrite $\Delta \boldsymbol{a}$ as follows:

$$\Delta \boldsymbol{a} = \sum_{k=0}^{n-1} \Delta a_{ok} \cdot \boldsymbol{x}_k \exp((\alpha_k + j\omega_k)t) \tag{31}$$

where Δa_{ok} is a constant and $\omega_k - j\alpha_k$ is the root of $\mu_k(\omega) = 0$.

Now we consider stability conditions for the oscillation mode. The oscillation mode represented by the eigenvector $\boldsymbol{x}_m$ is stable if one of following conditions is satisfied:

1) $\alpha_m < 0$ and $\alpha_k < 0$

2) $\alpha_m = 0$ and $\alpha_k < 0$

where $k = 1, 2, \cdots, m-1, m+1, m+2, \cdots, n-1$.

Condition 1) is obvious from (31) and the discussion in Section III. Condition 2) comes from the following considerations. The $\boldsymbol{x}_m$ component of $\Delta \boldsymbol{a}$ does not have influence on the stability of the oscillation mode $\boldsymbol{x}_m$ because it does not change the phase relation among the components of the vector $\boldsymbol{x}_m$. On the other hand, if a component other than the $\boldsymbol{x}_m$ component of $\Delta \boldsymbol{a}$ does not decrease with time, the oscillation mode $\boldsymbol{x}_m$ becomes unstable because the phase relation among the components of $\boldsymbol{x}_m$ cannot be kept. Further, the oscillation mode $\boldsymbol{x}_m$ becomes more stable as the $|\alpha_k|$ is greater.

V. Application to the Power-Combining System

Here, we apply the above stability condition to a power-coupling system of identical oscillators using hybrid couplers.

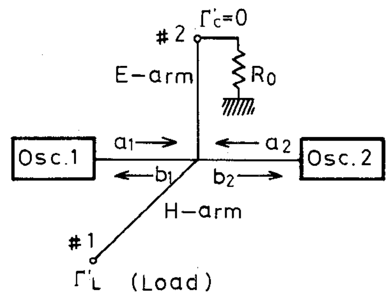

Fig. 8. Power-combining system of two identical oscillators using the magic-T.

A. Two-Oscillator System

Fig. 8 shows a power-combining system of two identical oscillators using the magic T. The scattering matrix $\boldsymbol{S}_L$ represents the coupled circuit and is given by

$$\boldsymbol{S}_L(\omega) = (\Gamma_L(\omega)/2) \begin{bmatrix} 1 & 1 \\ 1 & 1 \end{bmatrix} \tag{32}$$

where $\Gamma_L(\omega) = \Gamma_L'(\omega) \cdot e^{-j2\omega l/v}$, where l represents the equivalent length between the oscillator and the load, and v indicates the velocity of the wave.

The scattering matrix $\boldsymbol{S}_G$ represents a diagonal matrix with its diagonal components equal to the Rieke diagrams of oscillators. It follows from (32) that the amplitude of input wave b_1 is equal to that of b_2. Therefore, $\boldsymbol{S}_G$ is given by

$$\boldsymbol{S}_G(\boldsymbol{B}_o, \omega_o) = \begin{bmatrix} S_G^{\langle 1 \rangle}(\boldsymbol{B}_o, \omega_o) & 0 \\ 0 & S_G^{\langle 2 \rangle}(\boldsymbol{B}_o, \omega_o) \end{bmatrix}. \tag{33}$$

The operating points $S_G(B_o, \omega_o)$ and oscillation modes $\boldsymbol{x}$ of the circuit shown in Fig. 8 are given by calculating (23). We obtain

(A) $S_G^{\langle 1 \rangle}(B_o, \omega_o) = S_G^{\langle 2 \rangle}(B_o, \omega_o)$

(A.1) $S_G^{\langle 1 \rangle}(B_o, \omega_o) = S_G^{\langle 2 \rangle}(B_o, \omega_o) = \Gamma_L(\omega_o)$

$$\boldsymbol{x}_0 = (1, 1)^T \tag{34a}$$

(A.2) $S_G^{\langle 1 \rangle}(B_o, \omega_o) = S_G^{\langle 2 \rangle}(B_o, \omega_o) = 0$

$$\boldsymbol{x}_1 = (1, -1)^T \tag{34b}$$

(B) $S_G^{\langle 1 \rangle}(B_o, \omega_o) \neq S_G^{\langle 2 \rangle}(B_o, \omega_o)$

(B.1) $1/S_G^{\langle 1 \rangle}(B_o, \omega_o) + 1/S_G^{\langle 2 \rangle}(B_o, \omega_o) = 2/\Gamma_L(\omega_o)$

$$\boldsymbol{x}_h = \left(1/S_G^{\langle 1 \rangle}(B_o, \omega_o), 1/S_G^{\langle 2 \rangle}(B_o, \omega_o)\right)^T. \tag{34c}$$

For a small perturbation, the matrix $\boldsymbol{S}_N(\omega)$ as shown in (30) becomes

$$\boldsymbol{S}_N(\omega) = \begin{bmatrix} u^{\langle 1 \rangle} - \Gamma_L(\omega)/2 & -\Gamma_L(\omega)/2 \\ -\Gamma_L(\omega)/2 & u^{\langle 2 \rangle} - \Gamma_L(\omega)/2 \end{bmatrix}. \tag{35}$$

where $u^{\langle i \rangle} = S_o^{\langle i \rangle} + S_{G\omega o}^{\langle i \rangle} \cdot (\omega - \omega_o)$. From now on, $\Gamma_L(\omega)$ will be expressed approximately in the vicinity of the point $\Gamma_L(\omega_o)$ $(= \Gamma_o)$ as follows:

$$\Gamma_L(\omega) = \Gamma_o + \Gamma_{L\omega o} \cdot (\omega - \omega_o). \tag{36}$$

1) Oscillation Mode Given by (34a): In this case, the oscillators operate in the same phase. Therefore, this oscillation mode will be called the even mode. For the even mode, the output waves are represented by $\boldsymbol{a}_o = a_o \boldsymbol{x}_o$, where a_o is a constant indicating the output-wave amplitude. This is the desired oscillation mode because the coupling circuit delivers the summed output power to the load Γ_L. The eigenvectors $\boldsymbol{x}$ and associated eigenvalues λ of $\boldsymbol{S}_N$ are obtained as follows:

$$\lambda_0 = (S_{G\omega o} - \Gamma_{L\omega o})\cdot(\omega - \omega_o) \text{ for } \boldsymbol{x}_0$$
$$\lambda_1 = S_o + S_{G\omega o}\cdot(\omega - \omega_o) \text{ for } \boldsymbol{x}_1 \quad (37)$$

where the eigenvectors $\boldsymbol{x}_0$ and $\boldsymbol{x}_1$ are represented in (34). Equation (37) shows that the behavior of the $\boldsymbol{x}_0$ and $\boldsymbol{x}_1$ components of $\Delta\boldsymbol{a}$ are analyzed the same as Δa, respectively, of the oscillator terminated by a load and the injection-locked oscillator in Section III. From the stability condition 2) in Section IV, we easily find that when the reflection coefficient of the load is located in the stable region as shown in Fig. 3, the even mode $\boldsymbol{x}_0$ is stable because $\alpha_0 = 0$ and $\alpha_1 < 0$. The even mode becomes more stable because $|\alpha_1|$ becomes greater as the operating point S_o is located farther from the boundary line shown in Fig. 3.

2) Stability of Oscillation Mode Given by (34b): In this case, the oscillators operate in anti-phase. Therefore, this oscillation mode will be called the odd mode. For the odd mode, the output waves are represented by $\boldsymbol{a}_o = a_o \boldsymbol{x}_1$, where a_o is a constant indicating the output-wave amplitude. This is the undesired oscillation mode because the coupling circuit does not deliver the summed output power to the load Γ_L.

For this mode, $\boldsymbol{S}_N$ is given by (35) in which S_o is replaced by 0. The eigenvectors $\boldsymbol{x}$ and associated eigenvalues λ of $\boldsymbol{S}_N$ are obtained as follows:

$$\lambda_0 = (S_{G\omega o} - \Gamma_{L\omega o})\cdot(\omega - \omega_o) \text{ for } \boldsymbol{x}_0$$
$$\lambda_1 = S_{G\omega o}\cdot(\omega - \omega_o) \text{ for } \boldsymbol{x}_1. \quad (38)$$

Equation (38) shows that α_0, as well as α_1, is equal to 0. From the stability condition 2) in Section IV, the odd mode $\boldsymbol{x}_1$ is found to be unstable. In other words, this mode cannot exist in the system shown in Fig. 8.

3) Stability of Oscillation Mode Given by (34c): In this case, some oscillators take the operating points in the unstable region shown in Fig. 3. Therefore, this oscillation mode will be called the H-mode (hybrid-mode). For the H-mode, the output waves are represented by $\boldsymbol{a}_o = a_o \boldsymbol{x}_h$, where a_o is a constant indicating the output-wave amplitude. The H-mode is an undesired mode because the coupling circuit does not deliver the summed output power to the load Γ_L.

Here, let us assume that the operating points $S_G^{\langle 1\rangle}(B_o, \omega_o)$ and $S_G^{\langle 2\rangle}(B_o, \omega_o)$ are represented by $S_G^{\langle s\rangle}(B_o, \omega_o)$ and $S_G^{\langle u\rangle}(B_o, \omega_o)$, respectively. Then the eigenvalues λ_{h0} and λ_{h1} and the eigenvectors $\boldsymbol{x}_{h0}$ and $\boldsymbol{x}_{h1}$ are obtained as shown in the Appendix. Note that when $\omega \to \omega_o$, the directions of $\boldsymbol{x}_{h0}$ and $\boldsymbol{x}_{h1}$ become equal to those of $\boldsymbol{x}_h$ and $(1/(S_o^{\langle u\rangle}), -1/S_o^{\langle s\rangle})^T$, respectively. Then we find that the

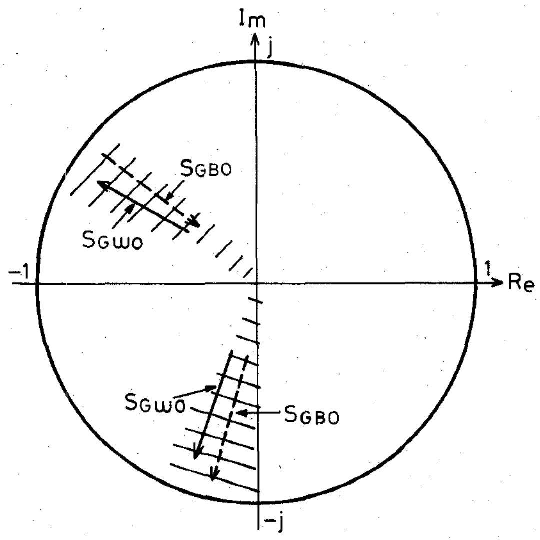

Fig. 9. Rieke diagram at port 1 of Fig. 8 when oscillators are in the H-mode (calculated from the Rieke diagram shown in Fig. 3).

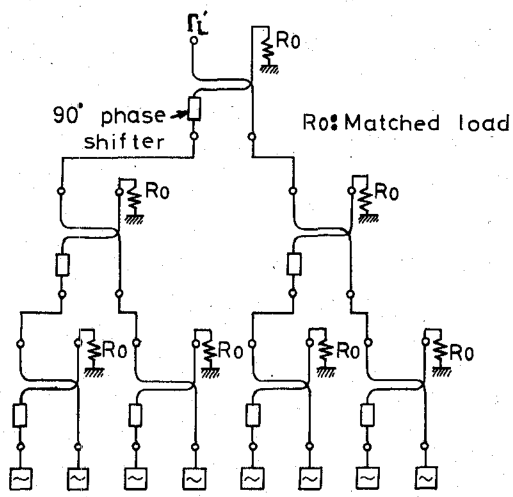

Fig. 10. Power-combining system of 2^3 identical oscillators system using 3-dB directional couplers.

H-mode $\boldsymbol{x}_h$ is stable because $\alpha_{h0} = 0$ and $\alpha_{h1} \leqslant 0$, where $-\alpha_{h0}$ and $-\alpha_{h1}$ are the imaginary parts of the roots of $\lambda_{h0}(\omega) = 0$ and $\lambda_{h1}(\omega) = 0$, respectively. Thus, it is found that the H-mode is harmful to single-mode operation. However, the effect of the H-mode is not very serious in the multiple-oscillator system for the following reasons.

1) In the H-mode, operating points occur in a narrow region, as shown in Fig. 9. This region can be avoided (Fig. 9 shows that when Γ_L is located outside the shaded area, oscillators cannot oscillate in the H-mode).

2) In the circuit for 2^n oscillators, only one oscillator can take the operating point in the unstable region, as we shall see in the next section.

B. 2^n Oscillators System

The above discussions can be extended to the 2^n identical oscillators system [7] as shown in Fig. 10. $\boldsymbol{S}_G$ is a $2^n \times 2^n$ diagonal matrix and is given by

$$\boldsymbol{S}_G(B_o, \omega) = \text{diag}\left[\cdots, S_G^{\langle i\rangle}(B_o, \omega), \cdots\right] \quad (39)$$

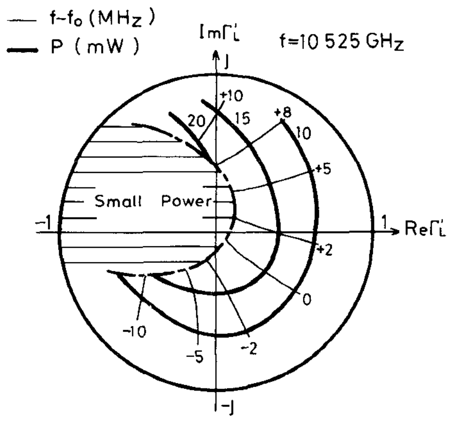

Fig. 11. Rieke diagram measured at port 1 of Fig. 8.

where $S_G^{\langle i\rangle}(B_o,\omega)$ is either $S_G^{\langle s\rangle}(B_o,\omega)$ or $S_G^{\langle u\rangle}(B_o,\omega)$. S_L is a $2^n \times 2^n$ matrix and all components are $\Gamma_L/2^n$.

The even mode x_0 and the odd modes $x_k(k=1,2,\cdots,2^n-1)$ are given by

$$x_m = \left(1, e^{jma}, \cdots, e^{jm(i-1)a}, \cdots, e^{jm(2^n-1)a}\right)^T \quad (40)$$

where $a=2\pi/2^n$ and $m=0,1,2,\cdots,2^n-1$. The similar analysis as shown in Section V-A can be applied, and we find that the even mode x_0 is stable and the odd modes x_k are unstable.

Next, we consider the H-modes. Suppose the number of oscillators whose operating points are in the unstable region is M, and then we obtain from $\det[S_N(\omega)]=0$

$$\left(S_G^{\langle s\rangle}\right)^{2^n-M-1}\left(S_G^{\langle u\rangle}\right)^{M-1}\left[\left(S_G^{\langle s\rangle}\right)\left(S_G^{\langle u\rangle}\right) - \left\{(2^n-M)S_G^{\langle u\rangle} + M\cdot S_G^{\langle s\rangle}\right\}\Gamma_L/2^n\right]=0. \quad (41)$$

When $M \geqslant 2$, this system becomes unstable because includes $S_G^{\langle u\rangle}=0$ (refer to Section III). Therefore, we can say that more than one oscillator cannot take the operating point which is located in the unstable region. Thus, even if one oscillator, unfortunately, takes the operating point in the unstable region, the output-wave vector a_o becomes

$$a_o = a_o\left(1,1,1,\cdots,1,1,S_G^{\langle u\rangle}/S_G^{\langle s\rangle},1,1,\cdots,1\right)^T. \quad (42)$$

Equation (42) indicates that as the number of oscillators is increased, the H-modes resemble the desired mode (the even mode) more closely and then the effect of the H-mode decreases.

The above mathematical results explain that the oscillators in Fig. 10 can be mutually locked in the even mode, and this system can give stable operation free from moding problems.

C. Experimental Results

Fig. 11 shows the Rieke diagram which was measured from port 1 of Fig. 8. Two identical Gunn oscillators with Rieke diagrams as shown in Fig. 2 were used.

Referring to Fig. 11, we find that the coupling circuit of Fig. 8 delivers the summed output power to the load when Γ_L, the reflection coefficient of the load, is located outside the shaded area in Fig. 11. On the other hand, the output power is small when Γ_L is located in the shaded area. This means that the oscillation mode x_0 dominates outside the shaded area, while the oscillation mode x_1 dominates in the shaded area. (Note that the oscillation mode x_1 can exist in the practical circuit because port 2 of Fig. 8 is slightly mismatched.)

If we rotate Fig. 11 about $\pi/4$ rad in the counterclockwise direction, then we find it resembles Fig. 2. The small power region corresponds to the unstable region of Fig. 2, and the output power is almost doubled in the stable region of Fig. 2. Therefore, we can say that the discussions in Section III are experimentally verified.

Furthermore, the experiments performed at about 30 MHz on the system with 16 tunnel-diode oscillators and lumped-constant 3-dB directional couplers as shown in Fig. 10 showed that the output power was multiplied by approximately 16, the spectrum was clean, and the circuit adjustment was easy [7]. Therefore, we can say that the oscillators were mutually locked in the even mode. These experimental results agree well with the analytical results in Section V-B.

VI. Conclusion

Using the Rieke diagram in terms of traveling waves, we have discussed the stability of the oscillation mode in a multiple-oscillator system. Further, we have clarified the conditions for a stable operation free from the mode problem as follows.

1) For the desired oscillation mode, the operating points must be located in the stable region of the Rieke diagram. Further, it is to be desired that the operating point is located farther from the boundary lines.

2) For the undesired oscillation modes, the oscillators must be in free-running conditions.

3) H-modes exist under some load conditions. Therefore, some procedure is needed to render this mode unstable or nondetrimental.

Appendix

For the H-mode, the eigenvalues λ_{h0} and λ_{h1}, and the eigenvectors x_{h0} and x_{h1} of the matrix S_N are given by

$$\begin{matrix}\lambda_{h0}\\ \lambda_{h1}\end{matrix} = \Big\{S_G^{\langle s\rangle}(B_o,\omega)+S_G^{\langle u\rangle}(B_o,\omega)-\Gamma_L(\omega) \mp\sqrt{\left(S_G^{\langle s\rangle}(B_o,\omega)-S_G^{\langle u\rangle}(B_o,\omega)\right)^2+\left(\Gamma_L(\omega)\right)^2}\Big\}/2 \quad (A1)$$

$$\begin{matrix}x_{h0}\\ x_{h1}\end{matrix} = \Big(\Gamma_L(\omega),\, S_G^{\langle s\rangle}(B_o,\omega)-S_G^{\langle u\rangle}(B_o,\omega) \pm\sqrt{\left(S_G^{\langle s\rangle}(B_o,\omega)-S_G^{\langle u\rangle}(B_o,\omega)\right)^2+\left(\Gamma_L(\omega)\right)^2}\Big)^T. \quad (A2)$$

When $\omega-\omega_o \to 0$, these become

$$\lambda_{h0} = \frac{\omega-\omega_o}{\left(S_o^{\langle s\rangle}\right)^2+\left(S_o^{\langle u\rangle}\right)^2} \times\Big\{\left(S_o^{\langle u\rangle}\right)^2 S_{G\omega o}^{\langle s\rangle}+\left(S_o^{\langle s\rangle}\right)^2 S_{G\omega o}^{\langle u\rangle} -\left(S_o^{\langle s\rangle}+S_o^{\langle u\rangle}\right)^2\Gamma_{L\omega o}/2\Big\} \quad (A3)$$

$$\lambda_{h1} = \frac{\left(S_o^{\langle s\rangle}\right)^2+\left(S_o^{\langle u\rangle}\right)^2}{S_o^{\langle s\langle}+S_o^{\langle u\rangle}} + \frac{\omega-\omega_o}{\left(S_o^{\langle s\rangle}\right)^2+\left(S_o^{\langle u\rangle}\right)^2}\Big\{\left(S_o^{\langle s\rangle}\right)^2 S_{G\omega o}^{\langle s\rangle}+\left(S_o^{\langle u\rangle}\right)^2 S_{G\omega o}^{\langle u\rangle} - \left(S_o^{\langle s\rangle}-S_o^{\langle u\rangle}\right)^2\Gamma_{L\omega o}/2\Big\} \tag{A4}$$

$$x_{h0} = 2\left(\frac{S_o^{\langle s\rangle}\cdot S_o^{\langle u\rangle}}{S_o^{\langle s\rangle}+S_o^{\langle u\rangle}}+\Gamma_{L\omega o}\cdot(\omega-\omega_o)/2,\ \frac{\left(S_o^{\langle s\rangle}\right)^2}{S_o^{\langle s\rangle}+S_o^{\langle u\rangle}} + \frac{\omega-\omega_o}{\left(S_o^{\langle s\rangle}\right)^2+\left(S_o^{\langle u\rangle}\right)^2}\Big\{\left(S_o^{\langle s\rangle}\right)^2 S_{G\omega o}^{\langle s\rangle}-\left(S_o^{\langle s\rangle}\right)^2 S_{G\omega o}^{\langle u\rangle} + \left(S_o^{\langle s\rangle}+S_o^{\langle u\rangle}\right)^2\Gamma_{L\omega o}/2\Big\}\right)^T \tag{A5}$$

$$x_{h1} = 2\left(\frac{S_o^{\langle s\rangle}\cdot S_o^{\langle u\rangle}}{S_o^{\langle s\rangle}+S_o^{\langle u\rangle}}+\Gamma_{L\omega o}\cdot(\omega-\omega_o)/2,\ -\frac{\left(S_o^{\langle u\rangle}\right)^2}{S_o^{\langle s\rangle}+S_o^{\langle u\rangle}} + \frac{\omega-\omega_o}{\left(S_o^{\langle s\rangle}\right)^2+\left(S_o^{\langle u\rangle}\right)^2}\Big\{\left(S_o^{\langle u\rangle}\right)^2 S_{G\omega o}^{\langle s\rangle}-\left(S_o^{\langle u\rangle}\right)^2 S_{G\omega o}^{\langle u\rangle} + \left(S_o^{\langle s\rangle}-S_o^{\langle u\rangle}\right)^2\Gamma_{L\omega o}/2\Big\}\right)^T. \tag{A6}$$

ACKNOWLEDGMENT

The author wishes to thank Prof. S. Mizushina of the Research Institute of Electronics at Shizuoka University and S. Katoh of Numazu College of Technology for their valuable comments and discussions.

REFERENCES

[1] C. T. Rucker, "A multiple-diode high-average power avalanche-diode oscillator," *IEEE Trans. Microwave Theory Tech.*, vol. MTT-17, p. 1156, Dec. 1969.

[2] K. Kurokawa and F. M. Magalhaes, "An X-band 10-W multiple-IMPATT oscillator," *Proc. IEEE*, vol. 59, pp. 102–103, Jan. 1971; also K. Kurokawa, "The single-cavity multiple-device oscillator," *IEEE Trans. Microwave Theory Tech.*, vol. MTT-19, pp. 793–800, Oct. 1971.

[3] R. S. Harp and H. L. Stover, "Power combining of X-band IMPATT circuit modules," presented at the 1973 IEEE Int. Solid-State Circuit Conf., Feb. 1973.

[4] M. Madihian and S. Mizushina, "A 3M-device cavity-type power combiner," *IEEE Trans. Microwave Theory Tech.*, vol. MTT-31, pp. 731–736, Sept. 1983.

[5] S. Mizushina, "2^n oscillators combined with 3-dB directional couplers for output power summing," *Proc. IEEE*, vol. 55, p. 2166, Dec. 1967.

[6] S. Mizushina, H. Kondoh, and M. Ashiki, "Corporate and tandem structures for combining power from 3^N and $2N+1$ oscillators," *IEEE Trans. Microwave Theory Tech.*, vol. MTT-28, pp. 1428–1432, Dec. 1980.

[7] S. Hamaya, "A single-mode parallel running system of 2^n oscillators," *Electron. Commun. Japan*, vol. 65-B, pp. 1377–1384, Nov. 1982.

[8] K. Kurokawa, "Injection locking of microwave solid-state oscillators," *Proc. IEEE*, vol. 61, pp. 1386–1410, Oct. 1973.

[9] Y. Okabe and S. Okamura, "Stability and noise of many oscillators in parallel running," *Electron. Commun. Japan*, vol. 53-B, pp. 743–751, Dec. 1970.

[10] S. Hamaya, "Graphical analysis of stability and noise of oscillator in several kinds of circuits," *Electron. Commun. Japan*, vol. 67-B, pp. 744–751, July 1984.

Susumu Hamaya (M'83) was born in Kanazawa, Japan, in 1943. He received the B.S. and the M.S. degrees in electronics engineering from Shizuoka University, Hamamatsu, Japan, in 1965 and 1967, respectively.

From 1967 to 1969, he was with the New Japan Radio Corporation, Mitaka, Japan. In 1969, he was a Research Assistant at Shizuoka University. In 1970, he joined the Numazu College of Technology, Numazu, Japan, where he is an Assistant Professor. He has worked on microwave solid-state devices, nonlinear waves, and computer software. His current research interests are concerned with microwave power-combining techniques, and the analysis and design of nonlinear microwave circuits.

Mr. Hamaya is a member of the Institute of Electronics and Communication Engineers of Japan.